Chemosphere 303 (2022) 135017

Contents lists available at ScienceDirect

Chemosphere

journal homepage: www.elsevier.com/locate/chemosphere

Natural solar activation of modified zinc oxides with rare earth elements (Ce, Yb) and Fe for the simultaneous disinfection and decontamination of urban wastewater

Ilaria Berruti [a], Nuno P.F. Gonçalves [c], Paola Calza [c], Maria Cristina Paganini [c], Isabel Oller [a,b], Maria Inmaculada Polo-López [a,b,*]

[a] CIEMAT-PSA, Carretera de Senés Km 4, 04200, Tabernas, Almería, Spain
[b] CIESOL, Joint Centre of the University of Almería-CIEMAT, 04120, Almería, Spain
[c] Department of Chemistry, Università di Torino, Via Giuria 7, 10125, Torino, Italy

HIGHLIGHTS

- Modified ZnO with Ce, Fe and Yb were photo-excited by natural sunlight
- Simultaneous disinfection and decontamination of urban wastewater was achieved
- Best performances were obtained with ZnO–Ce at 500 mg/L
- Organic matter and inorganic ions significantly affected process performance

GRAPHICAL ABSTRACT

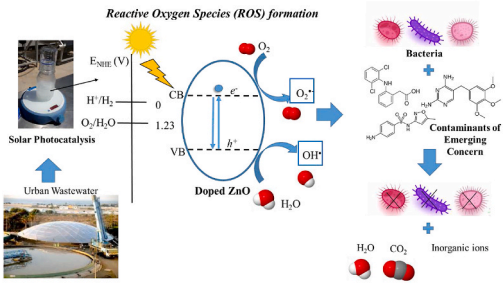

ARTICLE INFO

Handling Editor: CHANG MIN PARK

Keywords:
Bacteria
Contaminants of emerging concern
Heterogeneous photocatalysis
Solar energy
Urban wastewater

ABSTRACT

This study investigates the capability of modified zinc oxides (ZnO) with Ce, Yb and Fe towards the simultaneous inactivation of pathogenic bacteria (*Escherichia coli*, *Enterococcus faecalis* and *Pseudomonas aeruginosa*) and Contaminants of Emerging Concern (CECs, Diclofenac, Sulfamethoxazole and Trimethoprim) under natural sunlight. Several catalyst loads (from 0 to 500 mg/L) were assessed as proof-of principle in isotonic solution followed by the evaluation of organic matter effect in simulated and actual urban wastewater (UWW), using bare TiO_2–P25 as reference. The order of photocatalysts efficiency for both bacterial and CECs removal was: ZnO–Ce ≅ TiO_2–P25 > ZnO-Yb > ZnO–Fe > photolysis > darkness in all water matrices.

The best photocatalytic performance for water disinfection and decontamination was obtained with 500 mg/L of ZnO–Ce: 80% of ∑CECs removal after 45 min (4.4 kJ/L of accumulated solar UV-A energy (Q_{UV})) and the total inactivation of bacteria (Detection Limit of 2 CFU/mL) after 120 min (14 kJ/L of Q_{UV}) in UWW. The microbial and CECs abatement mechanism was described based on the generation of hydroxyl radicals, which was experimentally demonstrated for ZnO–Ce. Additionally, no significant release of Zn^{2+} and Ce was detected after the solar exposure. These results point out for the first time the capability of ZnO-Ce for the simultaneous UWW disinfection and decontamination under natural sunlight.

* Corresponding author. Plataforma Solar de Almería-CIEMAT, P.O. Box 22, 04200, Tabernas, Almería, Spain.
E-mail addresses: iberruti@psa.es (I. Berruti), nunopaulo.ferreiragoncalves@unito.it (N.P.F. Gonçalves), paola.calza@unito.it (P. Calza), mariacristina.paganini@unito.it (M.C. Paganini), ioller@psa.es (I. Oller), mpolo@psa.es (M.I. Polo-López).

https://doi.org/10.1016/j.chemosphere.2022.135017
Received 21 February 2022; Received in revised form 2 May 2022; Accepted 16 May 2022
Available online 21 May 2022

CRediT author statement

Ilaria Berruti: Formal analysis; Investigation; Writing – original draft. **Nuno P.F. Gonçalves**: Formal analysis; Writing – original draft. **Paola Calza:** Conceptualization; Project administration; Writing – review & editing. **Maria Cristina Paganini:** Conceptualization; Writing – review & editing. **Isabel Oller:** Supervision; Project administration; Writing – review & editing. **Maria Inmaculada Polo-López:** Supervision; Writing – review & editing.

1. Introduction

The anthropogenic activities have been progressively stressing the water quality by the continuous release of pollutants into the environment impacting aquatic biota with high risk for human health (UN-Water, 2019). To avert a global water crisis, the United Nations (UN) has made water protection one of the global priorities. By launching the international Water Decade Action (2018–2028) (United Nations, 2018), aligned with the Clean Water and Sanitation Sustainable Development Goal, UN aims to minimize the release of hazardous chemicals and materials, to reduce the untreated wastewater and to globally increase the recycling and safe water reuse, which requires efficient water treatment technologies.

Advanced oxidation processes (AOPs) have been attracting attention as a promising alternative to conventional water/wastewater treatment, such as the well-known UV-C radiation, ozonization, chlorination and filtration processes. AOPs are characterized by oxidation reactions mediated by the in situ generated highly reactive oxygen species (ROS) such as hydroxyl radicals ($HO^{\bullet}$) (Malato et al., 2009), able to react with a wide range of chemical compounds, and to eventually allow the achievement of the complete mineralization. Additionally, these ROS can effectively inactivate pathogens, such as bacteria, fungi, viruses and protozoa by oxidative stress. Among AOPs, heterogeneous photocatalysis, based on semiconductors, has being widely investigated as a promising method to lessen the water environmental problems (Byrne et al., 2018; Minella et al., 2017).

Photocatalysts' reaction mechanism is well known. During the photoexcitation of the semiconductor, electron-hole (e^-/h^+) pair is created between the valence band (VB) and the conduction band (CB). These photo-induced species can be trapped and recombined at the surface of the semiconductor, releasing energy in the form of heat. However, the h^+ and e^- reaction with oxygen and water molecules, respectively, leads to the formation of $HO^{\bullet}$ and superoxide radicals (Nosaka and Nosaka, 2017).

Among the most investigated semiconductors for water disinfection and decontamination, TiO_2–P25 is a reference material due to its non-toxic nature coupled with a low cost and its unique characteristics, such as wide bandgap in the near-UV spectral region, strong oxidation ability and very good photocatalytic properties (Byrne et al., 2018; Fagan et al., 2016). Nevertheless, ZnO has recently attracted the attention of the scientific community, due to its also unique characteristics including a wide band-gap at the solar near-UV spectrum (or larger absorption of the solar spectrum compared to TiO_2) (Ong et al., 2018), high oxidation and photocatalytic capability for organic detoxification and removal of pathogens from water and a large free-excitation binding energy, that permits its photoactivity at room temperature. ZnO is also odorless, water insoluble and relatively cheaper compared to TiO_2 (Lee et al., 2016).

On the other hand, one major drawback of bare photocatalysts (ZnO and TiO_2) is their low quantum efficiency, as a consequence of the very fast recombination of photogenerated electron-hole (e^-_{CB}/h^+_{VB}) pair created between the VB and the CB. The photocatalytic activity could be improved by enhancing the charge separation between h^+_{VB} and e^-_{CB} through heterojunction formation and introduction of doping agent (anionic, cation and rare earth dopants). The benefits of the doping agent rely on the fact that they may act as electron trapping agent to decrease the h^+_{VB} and e^-_{CB} recombination rate, leading to an increase in ROS generation and outperforming undoped bare photocatalysts performances. In the case of ZnO, several modification methods have been developed, in particular, the doping with certain cations and rare earth elements has shown to be promising (Khaki et al., 2017). The addition of transition metals, such us iron, was described to improve the ZnO efficiency under irradiation (Bousslama et al., 2017; Paganini et al., 2019). Similarly, the addition of low amounts of Ce or Yb was able to increase the photocatalytic efficiency for water disinfection and decontamination (Paganini et al., 2016; Zammit et al., 2018; Sordello et al., 2019; Cerrato et al., 2018a, 2020a). This effect has been explained by the formation of CeO_2 or Yb_2O_3 nanoparticles on larger ZnO nanostructures capable of promoting the bands alignment of the two different oxide phases and so helping the charge separation effect.

The application of semiconductors for water remediation can be even more favorable from an environmental perspective if combined with natural solar light, a renewable and free source of energy. The use of natural solar radiation to photoexcite semiconductors has been mainly focused on the use of TiO_2 (Agulló-Barceló et al., 2013; García--Fernández et al., 2015), although other semiconductors have also shown good water disinfection performances such as Ruana, PC500, Bi_2WO_6 (Helali et al., 2013), $Ag/BiVO_4$ (Booshehri et al., 2017) and TiO_2-graphene-oxide composites for water disinfection (Fernández-Ibáñez et al., 2015) and decontamination (Luna-Sanguino et al., 2021). Nevertheless, the attempt to simultaneously obtain water disinfection and decontamination by solar-driven photocatalytic semiconductors has been only marginally described so far in literature and mainly focused on the use of TiO_2–P25 (Grilla et al., 2019; Moreira et al., 2018). Under the author's knowledge there is a total absence of information in literature regarding the use of modified ZnO photocatalysts for simultaneous water disinfection and decontamination under natural sunlight.

Besides, photodegradation efficiency is also influenced by water composition. Commonly, complex water matrices negatively affect the efficiency of photocatalytic processes due to the presence of components that (*i*) serve as nutrients for bacteria, helping to maintain their viability, (*ii*) absorb photons competitively, (*iii*) act as scavengers of ROS, (*iv*) are absorbed on catalyst surface, inhibiting the material photoactivity. Moreover, water turbidity may hinder light transmission in the bulk of the solution and catalyst particles may aggregate in the presence of different ionic species (Rioja et al., 2016; Tsydenova et al., 2015).

The main goal of this study is the assessment of several modified ZnO photocatalysts with Ce, Yb or Fe, for water purification at lab-scale and under natural sunlight. The three prepared materials were fully characterized in previous works, showing preliminary promising activity under artificial visible light (lamp with maximum emission wavelength at 365 nm) for only pollutants abatement (Cerrato et al., 2018a; Paganini et al., 2019; Sordello et al., 2019). Therefore, the photoactivity performance of the same three ZnO photocatalysts has been evaluated herein for the first time toward the simultaneous removal of three CECs (namely Diclofenac-DCF, Sulfamethoxazole-SMX and Trimethoprim-TMP) and the inactivation of *E. coli*, *E. faecalis* and *P. aeruginosa*. The proof-of-principle of all photocatalysts in a wide range of concentration (0–500 mg/L) was investigated in isotonic water (IW), postulating the bacterial inactivation and CECs degradation mechanisms based on $HO^{\bullet}$ generation. Then, the potential influence of organic and inorganic chemical compounds commonly present in water matrices was also evaluated by performing tests in simulated (SUWW) and actual secondary effluent of urban wastewater (UWW). The performance efficiencies of the herein investigated photocatalysts have been analyzed in comparison with the benchmark TiO_2–P25, all of them used in suspension mode.

In addition, it is well-known that one of the main problems of ZnO is its stability, factor that is highly dependent on several factors, including the intensities of incident light, water pH, dissolved oxygen level and material properties. Higher intensities of incident light and ZnO, both very high and very low water pH values and oxygen-poor conditions produce higher ZnO dissolution rates, with release of Zn^{2+} (Taylor et al.,

2019). Therefore, the potential photo corrosion of the material, based on the release of Zn^{2+}, has been assessed in this study before and after the solar treatment.

2. Materials and methods

2.1. Water matrices

Three water matrices were used: (i) IW, (ii) SUWW and (iii) actual secondary effluent from the Municipal Wastewater Treatment Plant (UWW) of El Bobar in Almeria (Spain). IW was prepared with sterilized distilled water with NaCl 0.9% (w/v); the presence of salt was necessary to avoid osmotic bacterial stress. SUWW was used as synthetic model of municipal WW effluent (Polo-López et al., 2010). UWW was freshly collected and characterized by using pH meter (multi 720, WTW, Germany), conductivity meter (GLP31, CRISON, Spain) and turbidimeter (Model 2100 N, Hach, USA). Ionic composition was measured by ion chromatograph (Model 850, Metrohm, Switzerland). Dissolved Organic Carbon (DOC) was measured with a Total Organic Carbon (TOC) analyzer (Model 5050, Shimadzu, Japan). Table S1 (Supplementary material) shows the average values of the physicochemical and microbiological characterization of SUWW and UWW.

2.2. Contaminants of Emerging Concern (CECs) quantification

DCF, SMX and TMP were obtained from Sigma-Aldrich with high purity grade (>99%). They were selected due to their intensive use and low degradation in UWW effluents. The CECs were spiked in all water matrices from previously prepared stock solution containing each CEC at 8 mg/L in MilliQ water and stored at 4 °C, to reach an initial concentration of 100 μg/L each.

Each water sample (4.5 mL) was filtered through a 0.2 μm syringe-driven filter (Merck Millipore filter Hydrophobic (PTFE)), and washed with 0.5 mL of acetonitrile to remove any absorbed organic compounds. The concentration profiles of each CEC in water samples were monitored by UPLC/UV (Agilent Technologies, Series 1260), according to the following working conditions: A C-18 analytical column (Poroshell 120 EC -C18 3.0 × 50 mm 2.7 μm), 100 μL of injection volume and flow rate of 1 mL/min. The initial elution conditions were 95% water with 25 mM formic acid (mobile phase A) and 5% acetonitrile (mobile phase B). A linear gradient progressed from 5% of B to 90% in 12 min and then at 100% for 1 min. The re-equilibration time was 3 min with a flow of 1 mL/min. TMP, SMX and DCF were detected at 273, 267 and 285 nm with retention times of 2.5, 3.5 and 7.6 min, respectively.

2.3. Bacterial enumeration and quantification

Assays in IW and SUWW involved the use of three laboratory growing bacteria obtained from the Spanish Culture Collection (CECT); *E. coli* O157:H7 (CECT 4972), *E. faecalis* (CECT 5143) and *P. aeruginosa* (CECT 110).

E. coli was cultured in Nutrient-Broth Agar I (containing 5 g/L of beef extract (Panreac, Spain), 10 g/L of peptone (Panreac, Spain) and 5 g/L of NaCl (Sigma Aldrich)), *E. faecalis* in Luria Bertani Broth (Merck KGaA®, Darmstadt, Germany), and *P. aeruginosa* in Nutrient Broth No.2 ((Merck KGaA®, Darmstadt, Germany). They were incubated at 37 °C with agitation (at 100 rpm in a rotary shaking incubator) for 20 h. The suspensions yielded a concentration of ~10^9 CFU/mL and it was harvested by centrifugation for 15 min at 3000 rpm. Then, bacterial pellets were re-suspended in phosphate-buffered saline (PBS) solution and directly spiked in the reactors, filled with IW or SUWW, to obtain an initial concentration of 10^6 CFU/mL. Water samples from solar experiments were serial diluted in PBS and enumerated using the standard plate counting method. Briefly, 50 μL and 500 μL of samples (diluted or not) were spread on ChromoCult® Coliform Agar (Merck KGaA, Darmstadt, Germany), Pseudomonas Chromogenic Agar (Conda, Pronadisa, Spain) and Slanetz Bartley agar and incubated 24 h for *E. coli* (at 37 °C) and 48 h for *P. aeruginosa* (at 35 °C) and *E. faecalis* (at 37 °C). Detection limit (DL) was 2 CFU/mL.

For UWW experiments, naturally occurring *E. coli*, Total Coliforms, *Enterococcus* spp. and *Pseudomonas* spp. were evaluated. Bacterial concentration was obtained following the same standard plate counting methods explained above by spreading 50 μL and 500 μL of non-diluted water samples, reaching a similar DL.

2.4. Photocatalysts

The experiments were performed with three different ZnO materials with cerium (1%) (Ce), ytterbium (1%) (Yb) and iron (0.5%) (Fe) and the performances were compared with the benchmark TiO_2 Evonik P25. The preparation methods and characterization of each ZnO catalyst are reported elsewhere (Cerrato et al., 2018a; Paganini et al., 2019; Sordello et al., 2019). Briefly, they were synthetized starting from a 1 M water solution of $Zn(NO_3)_2 \bullet 6H_2O$ and kept under stirring in the presence of the stoichiometric amount of doping agent. The samples modified with 1% molar of rare earth elements, Ce and Yb, were prepared adding to the starting solution the corresponding precursor salts (nitrate) of Ce and Yb in stoichiometric amount, the sample modified with 0.5% molar of Fe was prepared starting from a solution of $FeCl_3$. Then a 4 M NaOH solution was added until the pH was 10–11. The solution was transferred into a PTFE lined stainless steel 100 mL autoclave (filling 70%) and treated at 175 °C overnight. The product was centrifuged and washed with deionized water, then dried at 70 °C. Scanning electron microscopy, transmission electron microscopy, X-rays powder diffraction, Brunauer–Emmett–Teller and diffuse reflectance DR-UV–vis characterization results of the used photocatalysts are reported in previous papers (Cerrato et al., 2020a, 2018a; Paganini et al., 2019), and summarized in Table S2.

The catalyst concentrations tested were 0, 100, 200 and 500 mg/L, selected according to previous studies, reporting an optimum concentration in this range for bacterial inactivation and CECs degradation with TiO_2–P25 (Agulló-Barceló et al., 2013; García-Fernández et al., 2015; Grilla et al., 2019). UV–visible absorbance profiles, measured by a spectrophotometer (UV–Vis Evolution 220, Thermo scientific), of the different photocatalysts at 100 mg/L are reported in Fig. S1 (Supplementary Material). The release of Zn^{2+} was analyzed by ICP-MS (iCAP TQ, Thermo Scientific) by an external service at University of Almeria (Spain).

2.5. Photocatalytic tests

The solar experiments were conducted in completely sunny days at Plataforma Solar de Almeria, Almeria, Spain (latitude: 37.0909°N, longitude: 2.357°W). 250-mL batch-vessels (DURAN Glass, Schott, Germany), magnetically stirred (at 350 rpm) and covered by a glass cover (Schott) to allow the solar radiation entering from all directions, were used to assess photocatalysts efficiency. A total volume of 200 mL was irradiated with 0.0095 m^2 of illuminated surface.

The proper amount of photocatalyst was added to the water matrix and subsequently the CECs and microbial suspensions were simultaneously diluted to obtain the desired initial concentrations. After 5 min of homogenization in the dark, the first sample (t = 0 min) was taken and then the reactors were exposed to natural solar light for solar photocatalytic tests or kept in the dark for control tests. For all water matrices, the mere effect of solar radiation was also tested following similar operating conditions, but without the addition of photocatalyst. Experiments started between 10:30–11:00 a.m. local time lasting 180 min of solar radiation exposure. Water samples were taken at regular intervals for bacterial and CECs quantification. Water temperature and pH were monitored along the treatment time with a thermometer (Checktemp, Hanna, Spain) and a pH-meter (110-K, Horiba Laqua act). Temperature ranged between 24 and 40.9 °C and water pH was 7.5–8.5.

Solar UV-A irradiance (280–400 nm) was measured using a pyranometer (Kipp&Zonen, CUV5, Netherlands). Minimum and maximum values recorded along solar experiments were 33.4 and 50.5 W/m^2, respectively. These values were used to calculate the parameter $Q_{UV,}$ the accumulative UV energy per unit of volume (kJ/L) received in a photoreactor, according to the following equation (Eq. (1)) (Agulló-Barceló et al., 2013; Polo-López et al., 2010):

$$Q_{UV,n} = Q_{UV,n-1} + \frac{UV_n \cdot A_i \cdot \Delta t}{V_t \cdot 1000} \quad \text{(Eq.1)}$$

Where $Q_{UV,n}$ and $Q_{UV,n-1}$ are the UV-A energy accumulated per litre (kJ/L) at times n and n-1; UV_n is the average incident radiation per the irradiated area (W/m^2); Δt (s) is the experimental time of the sample ($\Delta t = t_n - t_{n-1}$); A_i is the illuminated area of system (m^2); and V_t (L) is the total volume of water.

Averaged profiles of T, pH and UV-A irradiance obtained along the solar experiments are presented in Fig. S2 (Supplementary material). Each operating condition was replicated at least three times and the data are presented as the average of replicates' results with the standard deviation as error bar.

2.6. Scavenger tests

Scavenger experiments were carried out under simulated sunlight in a COFOMEGRA Solarbox system (Italy) equipped with a Xenon arc lamp (1500 W) with glass filters, cutting the transmission of wavelengths below 340 nm. Tests were carried out in an air-saturated pyrex glass cells magnetically stirred (dimensions: 4.0 cm diameter and 2.5 cm height; cutoff at 295 nm), containing 5 mL of solution. SMX was chosen as a model substrate at 25 mg/L, while the concentration of photocatalyst was 50 mg/L (concentrations selected in order to obtain a low degradation during time permitting to observe a proper quenching effect). SMX concentration was measured by using an HPLC system 9300, and applying the following working conditions: C-18 analytical column (RP C18 LiChroCART® - LiChrosphere® with 5 μm particles), 50 μL of injection volume, 1 mL/min flow rate, H_3PO_4 4.4 mM/acetonitrile (75/25), 267 nm detection wavelength and 7.3 min of retention time.

The light irradiance on the cell from 295 to 400 nm was 26.6 ± 1.1 W/m^2. Methanol (MeOH) and tert-butanol (TBA), two well-known scavenger agents of $HO^\bullet$, at concentration of 0.1 M, were used to confirm the generation and involvement of this radical in bacterial inactivation and pollutant removal.

2.7. Kinetic analysis

Microbial inactivation data were fitted by different kinetic models according to their inactivation profiles, following mathematical expression reported elsewhere: Model 1: Chick's law for log-lineal decay and Model 2: a 'shoulder phase' given by constant bacteria concentration followed by a log-linear decrease (García-Fernández et al., 2015). Contaminants degradation obeys in all cases pseudo-first order kinetic. The pseudo-first order rate constant k (min^{-1}) is obtained by fitting the data with a linear regression and it corresponds to the slope of the regression line. The kinetic analysis was performed in the case of bacteria at the detection limit (2 CFU/mL) and for CECs, considering the removal of 80%, according to the Swiss UWW regulation (The Swis Federal Council, 1998).

3. Results and discussion

3.1. Dark assessment of ZnO materials

The viability of each bacterium (*E. coli*, *E. faecalis* and *P. aeruginosa*) and the adsorption of each CEC (TMP, SMX and DCF) in the presence of 500 mg/L of each ZnO photocatalyst were tested in the dark (Fig. S3, supplementary material). The concentration of the three bacteria remained almost constant along the contact time, with an averaged 0.5 ± 0.4 LRV (Logarithm Reduction Value) observed for the three bacteria in 120 min (Fig. S3a). For CECs, adsorption was not observed in any case. The results obtained in the dark demonstrated that the removal of the targets (bacteria and CECs) in the presence of ZnO materials under natural sunlight can be exclusively attributed to the action of solar photons and/or the acceleration effect provoked by the photocatalysts activity.

3.2. Photocatalytic activity of ZnO materials in isotonic water

The photocatalytic capability of all ZnO at different catalyst concentrations (100, 200 and 500 mg/L) under natural solar radiation was simultaneously investigated against all bacteria (Fig. 1a) and CECs removal (Fig. 1b). Besides, the effect of solar radiation over bacteria (solar only disinfection) and CECs (solar photolysis) was assessed. The degradation profiles of each bacterium and CEC are presented in Fig. S4 and S5, while Tables S3, S5 summarize the kinetic constants of each target (Supplementary material).

The effect of natural solar radiation on bacteria viability showed that DL (2 CFU/mL) was reached after 45, 75 and 90 min of solar exposure (6.2, 10.5 and 12.7 kJ/L of Q_{UV}) for *E. coli*, *P. aeruginosa* and *E. faecalis*, respectively. Therefore, all bacteria showed a significant inactivation under natural sunlight (Fig. S4a), mainly attributed to the synergistic effect of solar UV photons and water temperature. It is well accepted that solar photons absorption can promote the generation of intracellular ROS (such as $O_2^\bullet$, $HO^\bullet$ and $HO_2^\bullet$), that can attack DNA, proteins, lipids and enzymes, which accumulated damages eventually determine the cell death (Nelson et al., 2018). Thermal effects, as promoter of bacterial inactivation, become important only for values higher than 40–45 °C (Berney et al., 2006), which were not attained during our experiments (T < 40 °C), discarding water temperature as key factor on the bacterial inactivation. Direct photolysis of CECs could also play a key role in their degradation, but, as it was observed in Fig. S4b, only DCF undergoes degradation under sunlight (80% of removal after 87 min or 7.6 kJ/L of Q_{UV}), attributed to its photon absorption in the range 300–330 nm (Moreira et al., 2018), while, the concentration of SMX and TMP remained constant for 3 h of solar exposure.

The addition of the investigated photocatalysts enhanced both the bacterial inactivation kinetics and CECs degradation in comparison with the mere effect of sunlight (Fig. 1), obtaining in all cases > 5-LRV of bacteria and 80% CECs removal. The kinetic rates acceleration is attributed to the production of $HO^\bullet$, able to oxidize organic compounds and playing the key role on pollutants (chemical and microbiological) abatement by solar photocatalysis.

All ZnO-based catalysts showed similar trend regarding bacterial inactivation and CECs removal and comparable kinetics (Fig. 1a). The order of bacterial reactivity was: *P. aeruginosa* (gram-negative) ≅ *E. coli* (gram-negative) > *E. faecalis* (gram-positive). It is recognized that gram-positive bacteria are less susceptible to photocatalytic treatments due to a thicker membrane requiring therefore a larger number of radicals to attain complete inactivation (Marugán et al., 2010). Regarding CECs, the following reactivity order was obtained: TMP ≅ DCF > SMX. It could be explained considering the reactivity of the different CECs with $HO^\bullet$ formed during the treatment. In fact, Wols et al., reported second order kinetic constants for the reaction between the three CECs and $HO^\bullet$ equal to (8.2 ± 0.3)·10^9 M^{-1}s^{-1}, (8.0 ± 0.7)·10^9 M^{-1}s^{-1} and (6.3 ± 0.5)·10^9 M^{-1}s^{-1} for DCF, TMP and SMX, respectively (Wols et al., 2013), in line with the order of reactivity found in this study.

However, the disinfection and decontamination performance of each ZnO photocatalyst showed different behaviour (Fig. 1a and b) and the following order of decreasing efficiency was observed: ZnO–Ce > ZnO-Yb > ZnO–Fe. The three photocatalysts used in this study were previously characterized, and they showed similar values of band gap i.e., ZnO–Ce (3.273 eV), ZnO-Yb (3.284 eV) and ZnO–Fe (3.275 eV)

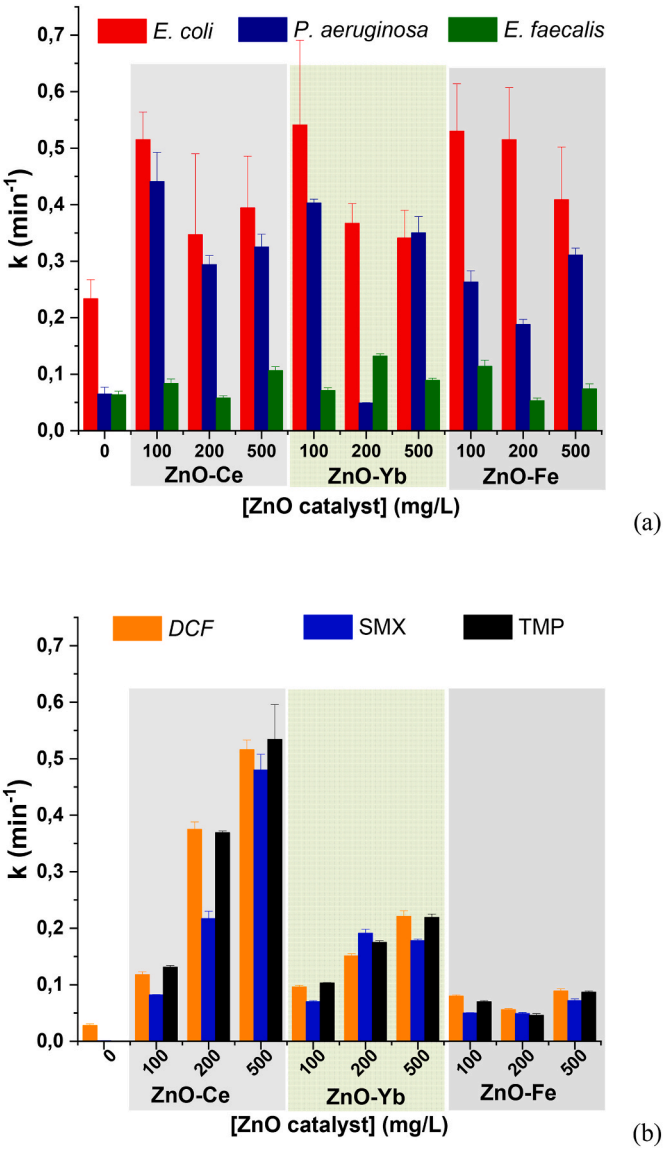

Fig. 1. (a) Inactivation kinetic constants of *E. coli*, *E. faecalis* and *P. aeruginosa* and (b) CECs degradation kinetic constants in the absence (0 mg/L) and presence of ZnO modified with Ce, Yb and Fe at concentrations of 100, 200 and 500 mg/L in IW under natural solar radiation.

(Table S2), demonstrating that the insertion of the dopant in the ZnO matrix did not dramatically affect the transition from the VB to CB of ZnO (Cerrato et al., 2018a).

Evidences of charge carrier generation and stabilization inside the solid particle were provided through Electron Paramagnetic Resonance (EPR) spectroscopy, giving a proof of material photoactivity and $HO^{\bullet}$ formation after excitation. EPR spectra, that could be observed in previous works (Cerrato et al., 2018a, 2018b, 2020a, 2020b, 2020b), showed the growth of EPR signal after irradiation, related to the stabilization of photoinduced charge carrier; the holes by oxygen ions (signal of the paramagnetic species O^{-}) and the electrons by specific cations, such as Zn^{2+} (signal of the paramagnetic species Zn^{+}). No significant differences related to the dopant ions (Ce, Yb and Fe) were observed in the EPR signal, but the relative growth of the EPR signals could give an insight on the operating mechanism in the different materials.

A schematic representation of the mechanism operating in the different catalysts is shown in Fig. 2. ZnO–Ce was reported to be a biphasic solid rather than a doped system (Cerrato et al., 2018a, 2018b, 2020a, 2018a) and the presence of a new crystalline phase, CeO_2, was assessed via XRD patterns and TEM (as it can be observed in micrographs previously reported (Cerrato et al., 2018a,b)). A growth of EPR signal was observed and it emerged that the number of trapped holes upon light irradiation was higher than that of trapped electrons, due to the presence of Ce^{4+}. According to reported DFT (Density Functional Theory) calculations, an electronic transition was possible from electrons photoexcited in ZnO CB to the empty and localized 4f levels of Ce^{4+}, that would be reduced to the paramagnetic species Ce^{3+} (not recorded), leading to a smaller number of visible photoexcited electrons to EPR technique (Cerrato et al., 2018b).

In the case of ZnO-Yb, a new crystalline phase formed (Yb_2O_3) was also detected, but it was lower and visible only by using a high resolution TEM technique (Cerrato et al., 2020a). Moreover, from EPR spectra it emerged that the amount of trapped electrons is higher than that of trapped holes (Cerrato et al., 2020a, 2020b). Unlike Ce, Yb has the 4f level fully occupied by electrons and consequently the electron transfer is prevented. In this case, Cerrato et al., suggested a hypothetical working mechanism based on the hole transfer, from ZnO VB to Yb_2O_3 VB, improving charge carrier separation (Cerrato et al., 2020a).

As regards, ZnO–Fe, iron ions entered in the structure of ZnO, without creating a new phase and a charge carrier separation could be made possible considering that the oxide CB has an energy close to the redox potential of the Fe^{3+}/Fe^{2+} pair. Fe^{3+} ion can be reduced to Fe^{2+} by the photogenerated electrons, according to the following reactions (R1-R4) (Paganini et al., 2019):

$$Fe^{3+} + e^{-}_{CB} \rightarrow Fe^{2+} \quad \text{(R1)}$$

$$Fe^{2+} + O_{2(ads)} \rightarrow Fe^{3+} + O_2^{-\bullet} \quad \text{(R2)}$$

$$Fe^{3+} + h^{+}_{VB} \rightarrow Fe^{4+} \quad \text{(R3)}$$

$$Fe^{4+} + OH^{-} \rightarrow Fe^{3+} + OH^{\bullet} \quad \text{(R4)}$$

According to the water disinfection and decontamination results obtained in this study, the most active sample was ZnO–Ce, and the faster results obtained could be explained considering the constitution of a significant heterostructure CeO_2–ZnO, that enhances the charge carrier separation leading to a larger amount of radicals generated in solution (Cerrato et al., 2018a). Besides, the participation of $HO^{\bullet}$ in the degradation of substrates by ZnO–Ce was confirmed experimentally through scavenger's experiments using SMX as target reference.

Fig. 3 shows SMX degradation curves ($C_0 = 25$ mg/L) in MilliQ water under simulated sunlight (photolysis), in the presence of ZnO–Ce at 50 mg/L, with or without MeOH and TBA at 0.1 M. SMX concentration, as it is reported before, remained constant under simulated sunlight, while an enhancement of its degradation was achieved in the presence of ZnO–Ce. In order to assess the role of $HO^{\bullet}$ in disinfection and decontamination of water, MeOH and TBA were added to the solution as efficient $HO^{\bullet}$ scavenger' species. Results demonstrated that SMX degradation after 30 min in the absence of scavengers was 70%, while in the presence of both MeOH and TBA no removal of SMX was observed, demonstrating the generation and the relevance of $HO^{\bullet}$ in the removal of this compound. Therefore, it can be concluded that the degradation and disinfection performance in the presence of ZnO–Ce may be attributed to the $HO^{\bullet}$ generation.

On the other hand, the use of a proper catalyst load is a requisite to attain the optimization of photocatalytic technologies performance based on semiconductors. The optimum load could vary in different systems due to the influence of several parameters that may play a (simultaneous) role, such as the optical properties (an efficient light absorption, and, therefore, smaller band gap values, could facilitates the generation of charge carriers in the photocatalyst, enhancing photocatalytic activity and requiring lower catalyst load to obtain better performances), amount of catalyst particles in suspension (related also with size of the particles), water path-length of photons (to avoid

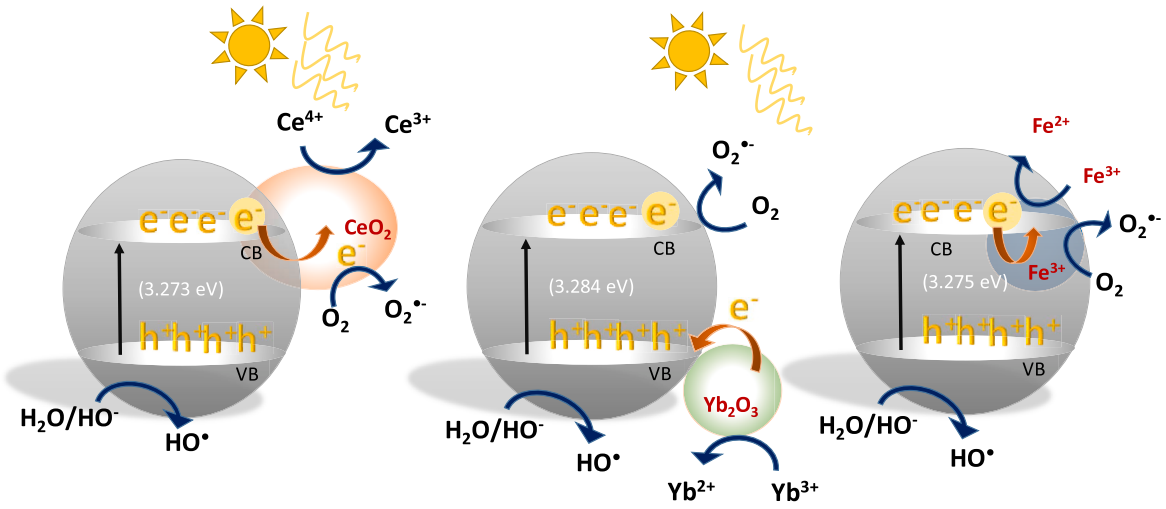

Fig. 2. Schematic representation of ROS generation by the modified ZnO with Ce, Yb and Fe in water and irradiated by natural solar radiation.

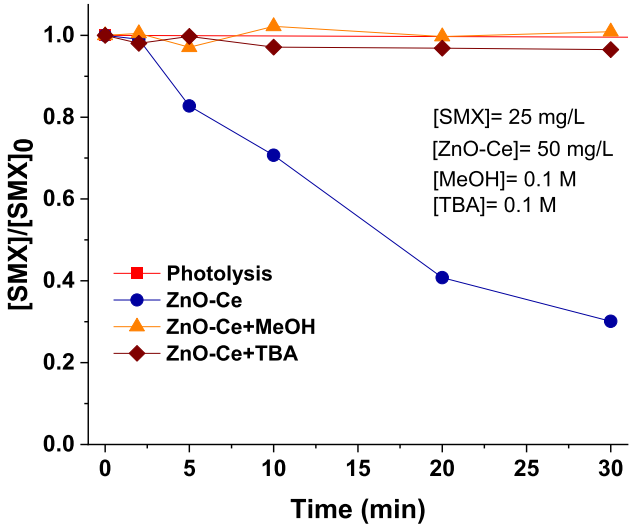

Fig. 3. SMX degradation curves (C_0 = 25 mg/L) under simulated sunlight (photolysis), in the presence of ZnO–Ce at 50 mg/L, with or without MeOH and TBA at 0.1 M.

absence of darkness areas), type of targets (microbial particles or dissolved organic, CECs) and complexity of the water matrices (Lee et al., 2016). The correct balance of all these parameters is crucial to finally obtain the maximum photocatalytic water treatment performance, as revealed also by the results obtained in this study.

Regarding the simultaneous water disinfection and decontamination, results showed that higher bacteria inactivation was achieved with 100 mg/L rather than 500 mg/L, while opposite results were obtained for CEC removal in IW (Fig. 1). This difference could be due to the higher catalyst concentration in solution, that may affect in different ways the bacterial cells and CECs: *i)* catalyst particles may have a shadowing or screening effect protecting bacteria from light (Helali et al., 2013); while *ii)* for CECs (dissolved substances), more catalyst means a higher number of active sites on the material and of photon absorption and, consequently, more electron-hole pairs generated and higher reaction rates. However, higher amount than an optimum leads also in contaminants degradation to a scattering effect, causing a decrease in the process efficiency (Abellán et al., 2009). This effect is independent from the type of catalyst, and similar behaviors observed herein for ZnO–Ce have been reported in the literature with other photocatalysts. Abellán et al., investigated the photocatalytic degradation of SMX and TMP by TiO_2 in a range of 0.1–2 g/L, showing that for concentrations >0.5 g/L, the degradation rate did not improve (Abellán et al., 2009). Helali et al., also showed that higher concentration than 0.5 g/L did not enhance the kinetic rate of *E. coli* in IW by TiO_2–P25, PC500, Ruana and Bi_2WO_6 photocatalysts, investigating a wide range of catalyst concentrations (0.05–1 g/L) (Helali et al., 2013). The disparity on optimal photocatalyts concentrations reported in literature, even when comparing performance with similar types of catalyst and geometrical reactors and at different concentrations, relies also on the fact that most of the studies investigated independently microorganisms and organic pollutants. The simultaneous analysis of both type of contamination clearly states that different concentrations are required to reach the best results, but for application in real scenarios the higher resistant pollutant should lately determine the optimal photocatalyst concentration.

In our study, the highest dosage of 500 mg/L was necessary for effectively address the simultaneous disinfection and decontamination in IW. At these conditions, DL for *E. coli*, *P. aeruginosa* and *E. faecalis* was attained within 60 min (6.5 kJ/L of Q_{UV}) and 80% removal of CECs in 3 min (0.4 kJ/L of Q_{UV}) of solar treatment time (Fig. S5).

3.3. Photocatalytic activity of ZnO materials in simulated urban wastewater

The performance of the different catalysts in SUWW under natural solar radiation was assessed for the simultaneous abatement of the three bacteria (Fig. 4a) and CECs (Fig. 4b), including also the benchmark TiO_2–P25 as reference. The kinetics data from the analysis of these results are described in Table S3 and S5; additionally, distinct inactivation and degradation profiles for all bacteria and CECs are shown in Fig. S6 and S7 (Supplementary material).

Concerning catalysts performance in SUWW, the best disinfection and decontamination efficiency was also obtained with ZnO–Ce at 500 mg/L. Under these conditions, DL was reached after 40, 50 and 120 min (3.8, 4.9 and 13.4 kJ/L of Q_{UV}) for *P. aeruginosa*, *E. coli* and *E. faecalis*, respectively, while 80% of CECs was removed in 37 min (3.6 kJ/L of Q_{UV}). Faster decontamination or degradation rate was not observed with any other ZnO tested, being therefore ZnO–Ce selected as potentially the best photocatalyst for a further investigation in UWW. Fig. 4 also shows that TiO_2–P25 was the most efficient photocatalyst for the degradation of CECs, but it exhibited a lower efficiency toward disinfection. In fact, 80% of total CECs were effectively removed after 19 min (1.6 kJ/L of Q_{UV}) both in the presence of 100 and 500 mg/L, but 120 min (13.5 kJ/L

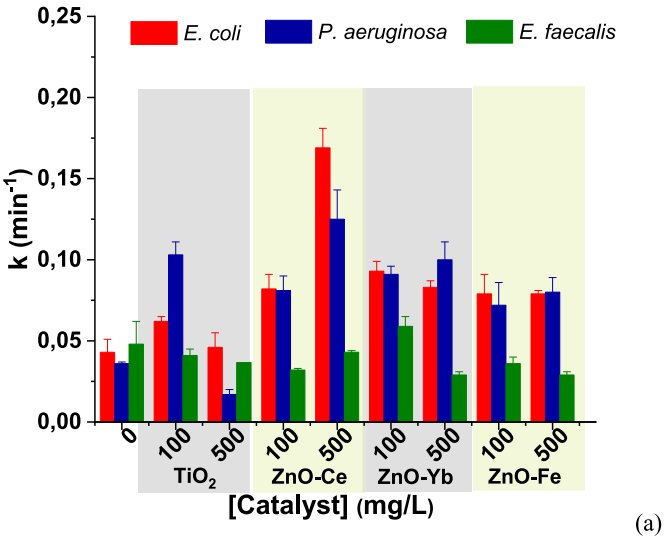

Fig. 4. (a) Inactivation kinetic constants of *E. coli*, *E. faecalis* and *P. aeruginosa* and (b) degradation constants of DCF, SMX and TMP in the absence (0 mg/L) and in the presence of ZnO modified with Ce, Yb and Fe and TiO_2–P25 at concentrations of 100 and 500 mg/L in SUWW under natural solar radiation.

of Q_{UV}) for *E. coli* and *P. aeruginosa* and 180 min for *E. faecalis* were necessary to reach DL at 500 mg/L. DOC was measured along all solar treatments, and results revealed that it remained almost constant at 20 mg/L (data not shown).

Microbial and CEC kinetic rates trend regarding reactivity order was similar than in IW: *P. aeruginosa* ≅ *E. coli* > *E. faecalis* and DCF > TMP > SMX. Although, in comparison with IW results, a reduction of 24% in efficiency was observed (kinetic constant 4 times lower in SUWW). It is well-known that the presence of inorganic ions and organic matter, acting as ROS scavengers and adsorbing on the catalyst surface, negatively affects the process performances, showing lower target removal efficiencies compared to pure water (Rioja et al., 2016).

3.4. Photocatalytic activity of ZnO–Ce and TiO_2–P25 materials in urban wastewater

Fig. 5a and b shows the inactivation kinetic constants of naturally occurring *E. coli*, Total Coliforms, *Enterococcus* spp. and *Pseudomonas* spp. and the inactivation profiles of the sum of all these bacteria, respectively, while Fig. 5c and d report degradation kinetic constants and total CECs degradation in UWW in the presence of ZnO–Ce and TiO_2–P25 at concentrations of 100 and 500 mg/L. Complementary profiles and kinetic analysis of each individual bacterium and CEC are shown in Fig. S8, S9 and Tables S4, S5 (supplementary material). The DOC concentration (ca. 22 mg/L) along the treatment time remained constant with all catalysts.

Fig. 5a and b shows that the better performance for water disinfection was obtained at 500 mg/L for both catalysts, at which DL for the sum of all bacteria was attained after 120 min (14 kJ/L of Q_{UV}). Nevertheless, at 100 mg/L of catalyst, a significant difference was observed between both catalysts, showing the greatest inactivation kinetics with ZnO–Ce. This effect could be correlated with the point of zero charge (PZC) of the two catalysts. At a typical pH of UWW (7.5–8), TiO_2 surface is negatively charged (PZC for TiO_2 is 6.2 (Chou and Liao, 2005)) and consequently, there would be repulsion between the negatively charged bacteria and TiO_2, resulting in a lower disinfection rate (Agulló-Barceló et al., 2013; Polo-López et al., 2010). PZC of modified ZnO is around 8.6–8.9 and positively-charged particles could show higher bactericidal activity, due to better adsorption of bacteria on the surface. Abbaszadegan et al., investigated the influence of different surface charges of silver nanoparticles (positive, neutral, and negative) on their antibacterial effectiveness against a panel of human pathogens, including gram-positive (i.e., *Staphylococcus aureus*, *Streptococcus mutans*, and *Streptococcus pyogenes*) and gram-negative (i.e., *E. coli*) bacteria. They showed that positively-charged silver nanoparticles had the highest bactericidal activity against all microorganisms tested (Abbaszadegan et al., 2014). Marugán et al., also emphasized the importance of bacteria adsorption on catalyst surface to effectively inactivate pathogens and reported disinfection rates significantly lower in the presence of Na_3PO_4 as a consequence of PO_4^{3-} adsorption on the surface, increasing bacterial repulsion (Marugán et al., 2010). Nevertheless, this effect is attenuated when increasing the catalyst concentration to 500 mg/L (Fig. 5a and b), due to the presence of a higher number of active sites and radicals simultaneously generated in the sample, reducing the influence of bacterial adsorption on the catalyst.

On the other hand, ZnO–Ce showed similar performance to TiO_2 for CECs removal in UWW. The best performance was clearly obtained at 500 mg/L of catalyst concentration (Fig. 5c and d); 80% removal of total CECs attained after 45 min (4.4 kJ/L of Q_{UV}) and 37 min (3.4 kJ/L of Q_{UV}), for ZnO–Ce and TiO–P25, respectively.

Despite of these results, ZnO–Ce is less influenced by this complex matrix than TiO_2 and a smaller decrease in the kinetic constants is shown (ratio k_{UWW}/k_{SUWW} closer to 1) (Fig. 6). This effect can be linked to the higher surface area of TiO_2 and the possible higher affinity towards natural organic matter (NOM), compared to ZnO- Ce . Consequently, removal of contaminants could be limited to the higher competition for the active sites between targets and NOM in the TiO_2 surface, in comparison with ZnO-Ce. However, further investigation is necessary to obtain experimental evidences on this matter. In the case of bacteria inactivation, the ratio between SUWW and UWW is not evaluated due to the potential significant different behaviour of culture (collection type-) and naturally occurring bacteria and this result could give uncertain and ambiguous conclusions.

It should be noted also that the removal remains the same in the different matrices (IW, SUWW and UWW), with SMX only exception as it was degraded with higher rates than TMP in UWW. The performances obtained in SUWW and UWW, showed that in UWW all kinetic rates were three/four times lower than in SUWW. This is mainly attributed to the more complex physicochemical and microbial scenario of UWW, where different family of pathogens and chemical species are simultaneously present, competing for catalyst actives sites and reactive species, as well as higher inorganic and organic matter content and turbidity, which finally determine lower reaction rates. Besides, it could be mentioned that, naturally occurring bacteria assessed in UWW have been described as more resistant to inactivation than commercial cultures (laboratory grown microorganisms) (García-Fernández et al.,

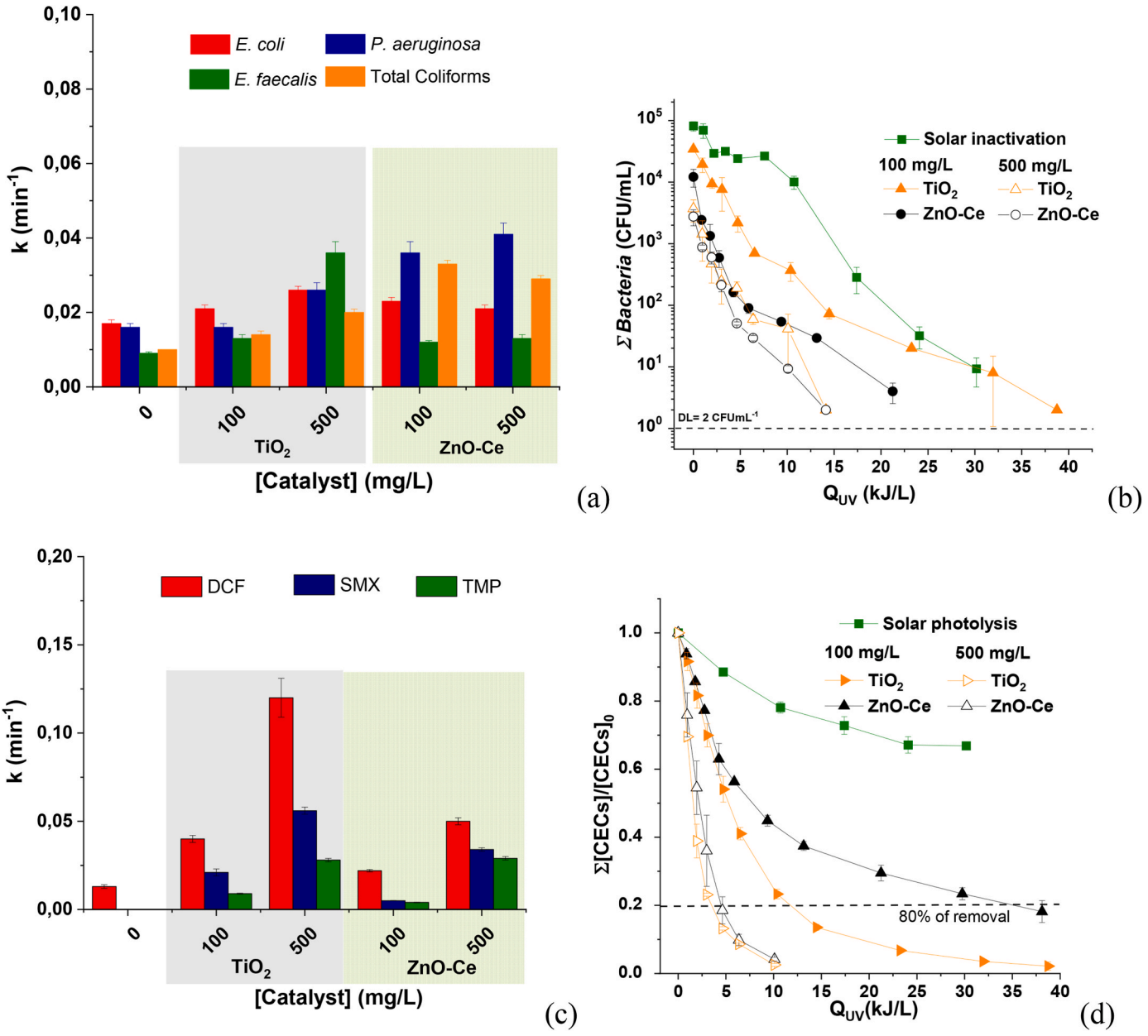

Fig. 5. (a) Inactivation kinetic constants of UWW natural occurring *E. coli*, Total coliforms, *Enterococcus* spp., and *Pseudomonas* spp., (b) inactivation bacteria summation profiles, (c) degradation kinetic constants of DCF, SMX and TMP and (d) total CECs degradation curves in the absence (0 mg/L) and presence of ZnO–Ce and TiO_2–P25 at concentrations of 100 and 500 mg/L under natural solar radiation.

2015). Concluding, it can be summarized that best results were found with ZnO–Ce at 500 mg/L, concentration that allows to remove 80% of the mixture of CECs after 45 min (4.4 kJ/L of Q_{UV}), while inactivation of wild bacteria present in UWW was achieved after 120 min (14 kJ/L of Q_{UV}), obtaining similar results with the benchmark TiO_2-P25.

Regarding literature, only few studies report on the successful photocatalytic efficiency of ZnO–Ce for water disinfection and decontamination. Zammit et al., demonstrated the inactivation of an isolated-UWW *E. coli* strain in IW under UV-A lamp (365 nm peak) with 100 mg/L after 135 min, exceeding the efficiency of the standard TiO_2–P25 in identical conditions (Zammit et al., 2018). Fabbri et al., studied the abatement of a cocktail of carbamazepine, atenolol, sulfamethoxazole, bisphenol A, diclofenac, ibuprofen and caffeine in MilliQ water and UWW, comparing the performances with TiO_2–P25. They reported higher removal efficiency for ZnO–Ce than TiO_2–P25 with 2 mg/L of each compound and 1 g/L of catalyst (Fabbri et al., 2019). Calza et al., investigated acesulfame K abatement by ZnO–Ce in ultrapure and river water under both UV–vis and visible light, emphasizing good performances of the semiconductor also in the presence of organic matter and under visible light (Calza et al., 2017). These previous works support the results obtained in the present study and demonstrate the capability of the ZnO photocatalyst with Ce for wastewater disinfection and decontamination.

Finally, it must be remarked that the use of ZnO particles could be a potential source of toxicity due to the release of Zn^{2+}. Therefore, the concentration of dissolved Zn^{2+} was analyzed by ICP-MS from samples containing 500 mg/L of ZnO–Ce exposed to natural sunlight and in the dark for 180 min, selected as the most stressful condition for the catalyst stability investigated in this study. The concentration detected was 1.70 mg/L and 3.63 mg/L for dark and sunlight, respectively; while the concentration of cerium in solution was negligible. The concentration of Zn^{2+} in natural waters is highly variable ranging from few μg/L to

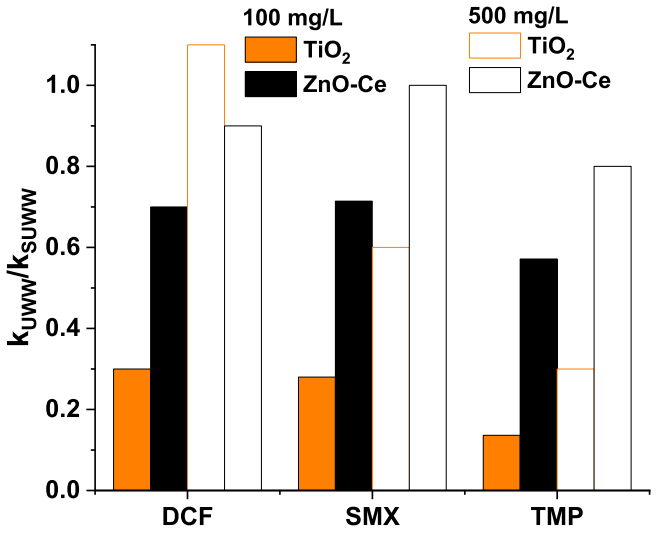

Fig. 6. Ratio between kinetic constants in UWW and SUWW of DCF, SMX and TMP in the presence of ZnO–Ce and TiO_2–P25 at concentrations of 100 and 500 mg/L.

several mg/L, attributed in some cases to the leaching from piping and fittings. Its maximum permissible concentration in potable water is 5 mg/L according to World Health Organization (WHO, 2011), similarly to the recommended concentration by the Environmental Protection Agency on National Secondary Drinking Water Regulations (USEPA, 2009). The concentration obtained in this study is lower than the established in guidelines and regulations, not considering therefore the employment of ZnO–Ce as a potential source of toxicity for human or environmental health. Nevertheless, and under the authors concern, in spite of the higher performance observed for the simultaneous water disinfection and decontamination at 500 mg/L of catalyst; 100 mg/L of ZnO–Ce photocatalyst load could be also selected as the most suitable concentration for UWW reclamation, based on two main criteria: (*i*) according to EU 2020/741 regulation (The European Parliament and the Council of the European Union, 2020), CECs removal is not included as water quality criteria, therefore considering only bacterial inactivation, 100 mg/L of ZnO–Ce is the optimal, considering similar performances than 500 mg/L, but requiring much lower catalyst load. (*ii*) A lower release of Zn^{2+} from 100 mg/L catalyst load is expected, which even would reduce any possible further toxic effects on the environment.

4. Conclusions

The feasibility of photocatalytic water treatments using modified ZnO with Ce, Yb and Fe has been demonstrated against several water-borne pathogens and CECs by exciting the semiconductors with natural solar radiation, an economically and ecologically source of light. Simultaneous water disinfection and decontamination were successful achieved in different water matrices including IW, SUWW and actual UWW. However, the modified photocatalysts ZnO–Fe and ZnO-Yb were discarded as potential efficient materials for an overall application in UWW purification due to low efficiencies obtained in SUWW in comparison with ZnO–Ce. Best results were found with ZnO–Ce at 500 mg/L, concentration that allows to remove 80% of the mixture of CECs after 45 min (4.4 kJ/L of Q_{UV}), while inactivation of wild bacteria present in UWW was achieved after 120 min (14 kJ/L of Q_{UV}), obtaining similar results with the benchmark TiO_2-P25.

The mechanism of bacterial inactivation and CECs degradation has been postulated for the modified photocatalyst of ZnO–Ce and attributed mainly to the hydroxyl radical's analysis performed in the sample and in the presence of SMX.

The release of Zn^{2+} ions during the irradiation time was below to the established in guidelines and regulations. Nevertheless, future research should be done focusing on the investigation of photocatalyst reuse and assessment of material photocorrosion in order to quantify the number of cycles to achieve good performances, without releasing Zn^{2+} in the environment.

Declaration of competing interest

The authors declare that they have no known competing financial interests or personal relationships that could have appeared to influence the work reported in this paper.

Acknowledgments

This work is part of a project that has received funding from the European Union's Horizon 2020 research and innovation programme under the Marie Skłodowska-Curie Grant Agreement No 765860 (AQUAlity).

Appendix A. Supplementary data

Supplementary data related to this article can be found at https://doi.org/10.1016/j.chemosphere.2022.135017.

References

Abbaszadegan, A., Ghahramani, Y., Gholami, A., Hemmateenejad, B., Dorostkar, S., Nabavizadeh, M., Sharghi, H., 2014. The effect of charge at the surface of silver nanoparticles on antimicrobial activity against gram-positive and gram-negative bacteria: a preliminary study abbas. J. Nanomater. 48, 395–400. https://doi.org/10.1155/2015/720654.

Abellán, M.N., Giménez, J., Esplugas, S., 2009. Photocatalytic degradation of antibiotics: the case of sulfamethoxazole and trimethoprim. Catal. Today 144, 131–136. https://doi.org/10.1016/j.cattod.2009.01.051.

Agulló-Barceló, M., Polo-López, M.I., Lucena, F., Jofre, J., Fernández-Ibáñez, P., 2013. Solar Advanced Oxidation Processes as disinfection tertiary treatments for real wastewater: implications for water reclamation. Appl. Catal. B Environ. 136–137, 341–350. https://doi.org/10.1016/j.apcatb.2013.01.069.

Berney, M., Weilenmann, H.U., Simonetti, A., Egli, T., 2006. Efficacy of solar disinfection of *Escherichia coli, Shigella flexneri, Salmonella Typhimurium* and *Vibrio cholerae*. J. Appl. Microbiol. 101, 828–836. https://doi.org/10.1111/j.1365-2672.2006.02983.x.

Booshehri, A.Y., Polo-Lopez, M.I., Castro-Alférez, M., He, P., Xu, R., Rong, W., Malato, S., Fernández-Ibáñez, P., 2017. Assessment of solar photocatalysis using Ag/$BiVO_4$ at pilot solar Compound Parabolic Collector for inactivation of pathogens in well water and secondary effluents. Catal. Today 281, 124–134. https://doi.org/10.1016/j.cattod.2016.08.016.

Bousslama, W., Elhouichet, H., Férid, M., 2017. Enhanced photocatalytic activity of Fe doped ZnO nanocrystals under sunlight irradiation. Optik 134, 88–98. https://doi.org/10.1016/j.ijleo.2017.01.025.

Byrne, C., Subramanian, G., Pillai, S.C., 2018. Recent advances in photocatalysis for environmental applications. J. Environ. Chem. Eng. 6, 3531–3555. https://doi.org/10.1016/j.jece.2017.07.080.

Calza, P., Gionco, C., Giletta, M., Kalaboka, M., Sakkas, V.A., Albanis, T., Paganini, M.C., 2017. Assessment of the abatement of acelsulfame K using cerium doped ZnO as photocatalyst. J. Hazard Mater. 323, 471–477. https://doi.org/10.1016/j.jhazmat.2016.03.093.

Cerrato, E., Gionco, C., Berruti, I., Sordello, F., Calza, P., Paganini, M.C., 2018a. Rare earth ions doped ZnO: synthesis, characterization and preliminary photoactivity assessment. J. Solid State Chem. 264, 42–47. https://doi.org/10.1016/j.jssc.2018.05.001.

Cerrato, E., Gionco, C., Paganini, M.C., Giamello, E., Albanese, E., Pacchioni, G., 2018b. Origin of visible light photoactivity of the CeO_2/ZnO heterojunction. ACS Appl. Energy Mater. 1, 4247–4260. https://doi.org/10.1021/acsaem.8b00887.

Cerrato, E., Zickler, G.A., Paganini, M.C., 2020a. The role of Yb doped ZnO in the charge transfer process and stabilization. J. Alloys Compd. 816, 152555. https://doi.org/10.1016/j.jallcom.2019.152555.

Cerrato, E., Paulo, N., Gonçalves, F., Calza, P., Paganini, M.C., 2020b. Comparison of the photocatalytic activity of ZnO/CeO_2 and ZnO/Yb_2O_3 mixed systems in the phenol removal from water: a mechanicistic approach. Catalysts 10, 1–15. https://doi.org/10.3390/catal10101222.

Chou, J.C., Liao, L.P., 2005. Study on pH at the point of zero charge of TiO_2 pH ion-sensitive field effect transistor made by the sputtering method. Thin Solid Films 476, 157–161. https://doi.org/10.1016/j.tsf.2004.09.061.

Fabbri, D., López-Muñoz, M.J., Daniele, A., Medana, C., Calza, P., 2019. Photocatalytic abatement of emerging pollutants in pure water and wastewater effluent by TiO_2 and Ce-ZnO: degradation kinetics and assessment of transformation products. Photochem. Photobiol. Sci. 18, 845–852. https://doi.org/10.1039/c8pp00311d.

Fagan, R., McCormack, D.E., Dionysiou, D.D., Pillai, S.C., 2016. A review of solar and visible light active TiO_2 photocatalysis for treating bacteria, cyanotoxins and contaminants of emerging concern. Mater. Sci. Semicond. Process. 42, 2–14. https://doi.org/10.1016/j.mssp.2015.07.052.

Fernández-Ibáñez, P., Polo-López, M.I., Malato, S., Wadhwa, S., Hamilton, J.W.J., Dunlop, P.S.M., D'Sa, R., Magee, E., O'Shea, K., Dionysiou, D.D., Byrne, J.A., 2015. Solar photocatalytic disinfection of water using titanium dioxide graphene composites. Chem. Eng. J. 261, 36–44. https://doi.org/10.1016/j.cej.2014.06.089.

García-Fernández, I., Fernández-Calderero, I., Polo-López, M.I., Fernández-Ibáñez, P., 2015. Disinfection of urban effluents using solar TiO_2 photocatalysis: a study of significance of dissolved oxygen, temperature, type of microorganism and water matrix. Catal. Today 240, 30–38. https://doi.org/10.1016/j.cattod.2014.03.026.

Grilla, E., Matthaiou, V., Frontistis, Z., Oller, I., Polo, M.I., Malato, S., Mantzavinos, D., 2019. Degradation of antibiotic trimethoprim by the combined action of sunlight, TiO_2 and persulfate: a pilot plant study. Catal. Today 328, 216–222. https://doi.org/10.1016/j.cattod.2018.11.029.

Helali, S., Polo-López, M.I., Fernández-Ibáñez, P., Ohtani, B., Amano, F., Malato, S., Guillard, C., 2013. Solar photocatalysis: a green technology for *E. coli* contaminated water disinfection. Effect of concentration and different types of suspended catalyst. J. Photochem. Photobiol. Chem. 276, 31–40. https://doi.org/10.1016/j.jphotochem.2013.11.011.

Khaki, M.R.D., Shafeeyan, M.S., Raman, A.A.A., Daud, W.M.A.W., 2017. Application of doped photocatalysts for organic pollutant degradation - a review. J. Environ. Manag. 198, 78–94. https://doi.org/10.1016/j.jenvman.2017.04.099.

Lee, K.M., Lai, C.W., Ngai, K.S., Juan, J.C., 2016. Recent developments of zinc oxide based photocatalyst in water treatment technology: a review. Water Res. 88, 428–448. https://doi.org/10.1016/j.watres.2015.09.045.

Luna-Sanguino, G., Ruíz-Delgado, A., Duran-Valle, C.J., Malato, S., Faraldos, M., Bahamonde, A., 2021. Impact of water matrix and oxidant agent on the solar assisted photodegradation of a complex mix of pesticides over titania-reduced graphene oxide nanocomposites. Catal. Today. https://doi.org/10.1016/j.cattod.2021.03.022.

Malato, S., Fernández-Ibáñez, P., Maldonado, M.I., Blanco, J., Gernjak, W., 2009. Decontamination and disinfection of water by solar photocatalysis: recent overview and trends. Catal. Today 147, 1–59. https://doi.org/10.1016/j.cattod.2009.06.018.

Marugán, J., van Grieken, R., Pablos, C., Sordo, C., 2010. Analogies and differences between photocatalytic oxidation of chemicals and photocatalytic inactivation of microorganisms. Water Res. 44, 789–796. https://doi.org/10.1016/j.watres.2009.10.022.

Minella, M., Fabbri, D., Calza, P., Minero, C., 2017. Selected hybrid photocatalytic materials for the removal of drugs from water. Curr. Opin. Green Sustain. Chem. 6, 11–17. https://doi.org/10.1016/j.cogsc.2017.05.002.

Moreira, N.F.F., Narciso-da-Rocha, C., Polo-López, M.I., Pastrana-Martínez, L.M., Faria, J.L., Manaia, C.M., Fernández-Ibáñez, P., Nunes, O.C., Silva, A.M.T., 2018. Solar treatment (H_2O_2, TiO_2-P25 and GO-TiO_2 photocatalysis, photo-Fenton) of organic micropollutants, human pathogen indicators, antibiotic resistant bacteria and related genes in urban wastewater. Water Res. 135, 195–206. https://doi.org/10.1016/j.watres.2018.01.064.

Nelson, K.L., Boehm, A.B., Davies-Colley, R.J., Dodd, M.C., Kohn, T., Linden, K.G., Liu, Y., Maraccini, P.A., McNeill, K., Mitch, W.A., Nguyen, T.H., Parker, K.M., Rodriguez, R.A., Sassoubre, L.M., Silverman, A.I., Wigginton, K.R., Zepp, R.G., 2018. Sunlight-mediated inactivation of health-relevant microorganisms in water: a review of mechanisms and modeling approaches. Environ. Sci. Process. Impacts 20, 1089–1122. https://doi.org/10.1039/c8em00047f.

Nosaka, Y., Nosaka, A.Y., 2017. Generation and detection of reactive oxygen species in photocatalysis. Chem. Rev. https://doi.org/10.1021/acs.chemrev.7b00161.

Ong, C.B., Ng, L.Y., Mohammad, A.W., 2018. A review of ZnO nanoparticles as solar photocatalysts: synthesis, mechanisms and applications. Renew. Sustain. Energy Rev. 81, 536–551. https://doi.org/10.1016/j.rser.2017.08.020.

Paganini, M.C., Dalmasso, D., Gionco, C., Polliotto, V., Mantilleri, L., Calza, P., 2016. Beyond TiO_2: cerium-doped zinc oxide as a new photocatalyst for the photodegradation of persistent pollutants. ChemistrySelect 1, 3377–3383. https://doi.org/10.1002/slct.201600645.

Paganini, M.C., Giorgini, A., Gonçalves, N.P.F., Gionco, C., Bianco Prevot, A., Calza, P., 2019. New insight into zinc oxide doped with iron and its exploitation to pollutants abatement. Catal. Today 328, 230–234. https://doi.org/10.1016/j.cattod.2018.10.054.

Polo-López, M.I., Fernández-Ibáñez, P., García-Fernández, I., Oller, I., Salgado-Tránsito, I., Sichel, C., 2010. Resistance of *Fusarium* sp spores to solar TiO_2 photocatalysis: influence of spore type and water (scaling-up results). J. Chem. Technol. Biotechnol. 85, 1038–1048. https://doi.org/10.1002/jctb.2397.

Rioja, N., Zorita, S., Peñas, F.J., 2016. Effect of water matrix on photocatalytic degradation and general kinetic modeling. Appl. Catal. B Environ. 180, 330–335. https://doi.org/10.1016/j.apcatb.2015.06.038.

Sordello, F., Berruti, I., Gionco, C., Paganini, M.C., Calza, P., Minero, C., 2019. Photocatalytic performances of rare earth element-doped zinc oxide toward pollutant abatement in water and wastewater. Appl. Catal. B Environ. 245, 159–166. https://doi.org/10.1016/j.apcatb.2018.12.053.

Taylor, C.M., Ramirez-Canon, A., Wenk, J., Mattia, D., 2019. Enhancing the photo-corrosion resistance of ZnO nanowire photocatalysts. J. Hazard Mater. 378, 120799. https://doi.org/10.1016/j.jhazmat.2019.120799.

The European Parliament and the Council of the European Union, 2020. Regulation (EU) 2020/741 of 25 May 2020 on Minimum Requirements for Water Reuse. Off. J. Eur. Union, 2019L 177/32-L 177/55.

The Swis Federal Council, 1998. Status as of 1 January 2021) Waters Protection Ordinance (WPO) 1–70.

Tsydenova, O., Batoev, V., Batoeva, A., 2015. Solar-enhanced advanced oxidation processes for water treatment: simultaneous removal of pathogens and chemical pollutants. Int. J. Environ. Res. Publ. Health 12, 9542–9561. https://doi.org/10.3390/ijerph120809542.

United Nations, 2018. United Nations Secretary-General's Plan: Water Action Decade 2018–2028. https://wateractiondecade.org/wp-content/uploads/2018/03/UN-SG-Action-Plan_Water-Action-Decade-web.pdf.

Un-Water, 2019. WWAP (UNESCO World Water Assessment Programme). United Nations Educational, Scientific and Cultural Organization, p. 201.

USEPA, 2009. Drinking water regulations and contaminants. URL. https://www.epa.gov/sdwa/drinking-water-regulations-and-contaminants.

WHO, 2011. Guidelines for Drinking-Water Quality, fourth ed. WHO Library Cataloguing-in-Publication Data. Available online: https://www.who.int/publications/i/item/9789241549950.

Wols, B.A., Hofman-Caris, C.H.M., Harmsen, D.J.H., Beerendonk, E.F., 2013. Degradation of 40 selected pharmaceuticals by UV/H_2O_2. Water Res. 47, 5876–5888. https://doi.org/10.1016/j.watres.2013.07.008.

Zammit, I., Vaiano, V., Iervolino, G., Rizzo, L., 2018. Inactivation of an urban wastewater indigenous: *Escherichia coli* strain by cerium doped zinc oxide photocatalysis. RSC Adv. 8, 26124–26132. https://doi.org/10.1039/c8ra05020a.